JOURNAL OF ELECTROMAGNETIC ENGINEERING AND SCIENCE, VOL. 16, NO. 1, 44~51, JAN. 2016

http://dx.doi.org/10.5515/JKIEES.2016.16.1.44
ISSN 2234-8395 (Online) · ISSN 2234-8409 (Print)

# 6–18 GHz Reactive Matched GaN MMIC Power Amplifiers with Distributed L-C Load Matching

Jihoon Kim* · Kwangseok Choi · Sangho Lee · Hongjong Park · Youngwoo Kwon

## Abstract

A commercial 0.25 μm GaN process is used to implement 6–18 GHz wideband power amplifier (PA) monolithic microwave integrated circuits (MMICs). GaN HEMTs are advantageous for enhancing RF power due to high breakdown voltages. However, the large-signal models provided by the foundry service cannot guarantee model accuracy up to frequencies close to their maximum oscillation frequency ($F_{max}$). Generally, the optimum output load point of a PA varies severely according to frequency, which creates difficulties in generating watt-level output power through the octave bandwidth. This study overcomes these issues by the development of in-house large-signal models that include a thermal model and by applying distributed L-C output load matching to reactive matched amplifiers. The proposed GaN PAs have successfully accomplished output power over 5 W through the octave bandwidth.

**Key Words**: 0.25 μm Gallium Nitride (GaN) Process, Distributed L-C, Large-Signal Model, Monolithic Microwave Integrated Circuit (MMIC), Wideband Power Amplifier.

## I. INTRODUCTION

A wideband RF power amplifier (PA) is an essential component in many RF applications, such as electronic warfare (EW) systems and security communications. In the past, the traveling wave tube amplifier (TWTA) has been most commonly used to achieve wideband output power above watt levels [1, 2]. However, the emergence of GaN PAs raises the prospect of replacing bulky TWTAs with compact solid state power amplifiers (SSPAs) [3]. GaN high-electron-mobility transistors (HEMTs) have several inherent advantages, including high breakdown voltage, high current density, and high saturation velocity resulting from their wide band gap properties [4]. Unfortunately, unlike GaAs or InP HEMTs, GaN HEMTs have a large power dissipation, which causes a prominent self-heating phenomenon that degrades the RF performance of devices [5]. Thus, the self-heating effect must be considered when designing wideband RF GaN PAs. An accurate large-signal model that includes a thermal model therefore becomes an inevitable requirement. Large-signal models provided by the foundry service are still not mature and do not guarantee model accuracy up to frequencies close to the maximum oscillation frequency ($F_{max}$). In-house large-signal modeling should definitely be performed, based on measured data.

The optimum output load point of an RF PA typically shows severe variation with the frequency. Because of this variation, a conventional output load matching prevents RF PAs from obtaining wideband output power. The output load matching circuits should therefore be designed by taking into consideration the frequency-dependent load variation.

This paper describes the development of in-house large-signal models of a GaN HEMT that include a thermal model.

Manuscript received November 7, 2015 ; Revised December 28, 2015 ; Accepted December 28, 2015. (ID No. 20151107-055J)
School of Electrical Engineering and Computer Science and INMC, Seoul National University, Seoul, Korea.
*Corresponding Author: Jihoon Kim (e-mail: j7h7@snu.ac.kr)

Distributed L-C output load matching is proposed for the design of reactive matched amplifiers. Section II presents the large-signal models, followed by the proposed design of the reactive matching PA in Section III. Experimental results are presented in Section IV.

## II. Large-Signal Modeling of the GaN HEMT

Our in-house models are based on an Angelov model [6, 7]. Fig. 1 shows an Angelov model-based GaN HEMT large-signal equivalent circuit including a thermal model. Our in-house models consist of the Angelov model library supported by Keysight's ADS 2013 program and thermal sub-circuits [8]. Thermal sub-circuits inform a temperature-dependent large-signal model of the channel temperature raised by $R_{th}$. In particular, our in-house models incorporate a nonlinear drain current ($I_{ds}$) that is divided into a nonlinear drain DC current (DC $I_{ds}$) and a nonlinear drain RF current (RF $I_{ds}$). This expression can make the $I_{ds}$ models reflect the frequency dispersion effect [9]. At high frequencies above a few megahertz, the RF $I_{ds}$ is activated through virtual inductances in the equivalent circuit model. Equations for the DC $I_{ds}$ are defined in (1)–(10). Each model parameter is optimized and fitted in comparison with measured DC–IV curves and *S*-parameters by ADS 2013. The RF $I_{ds}$ uses the same equation as the DC $I_{ds}$. Nonlinear capacitances ($C_{gs}$, $C_{gd}$, and $C_{ds}$) are fitted to well-known Angelov's nonlinear capacitance model equations [6].

$$\text{DC } I_{ds} = I_{pk0\_T}(1+\tanh(\psi)\tanh(\alpha V_{ds}))(1+\lambda V_{ds}) \quad (1)$$

$$I_{pk0\_T} = I_{pk0}(1+TCI_{pk0}(T-T_0)) \quad (2)$$

$$\psi = P_{1m}(V_{gs}-V_{pkm}) + V_{eff1} + V_{eff2} \quad (3)$$

$$P_{1m} = P_{1\_T}\left(1+\frac{B_1}{\cosh(B_2 V_{ds})^2}\right) \quad (4)$$

$$P_{1\_T} = P_1(1+\mathrm{TCP}_1(T-T_0)) \quad (5)$$

$$V_{pkm} = V_{pks} - DV_{pks}(1-\tanh(\alpha V_{ds})) \quad (6)$$

$$V_{eff1} = P_{21}\left(\frac{V_{gst}-V_{gsta}}{2}\right)^2 + P_{22}\left(\frac{V_{gst}+V_{gsta}}{2}\right)^2 \quad (7)$$

$$V_{eff2} = P_{31_{dc}}\left(\frac{V_{gst}-V_{gsta}}{2}\right)^3 + P_{32}\left(\frac{V_{gst}+V_{gsta}}{2}\right)^3 \quad (8)$$

$$\alpha = \mathrm{A}_1 + \mathrm{A}_2(1+\tanh(\psi)) \quad (9)$$

$$V_{gst} = V_{gs} - V_{pkm} \quad (10)$$

$$V_{gsta} = constant \quad (11)$$

Fig. 2 shows the large-signal modeling procedures. First, DC–IV curves are measured in a device under test (DUT) by an HP 4142B DC source and a Keysight's IC-CAP program. The

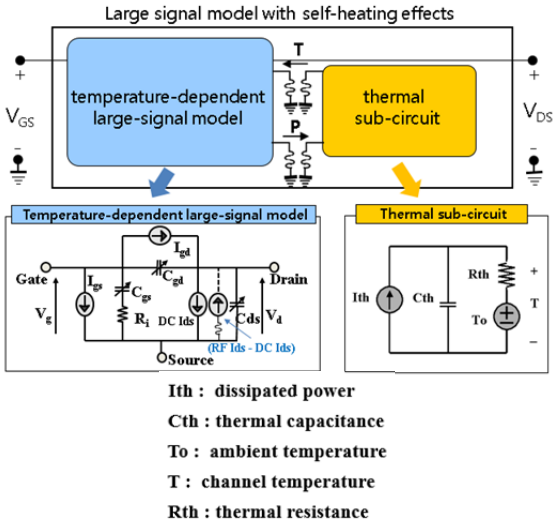


Fig. 1. Angelov model-based GaN HEMT large-signal model including thermal model.

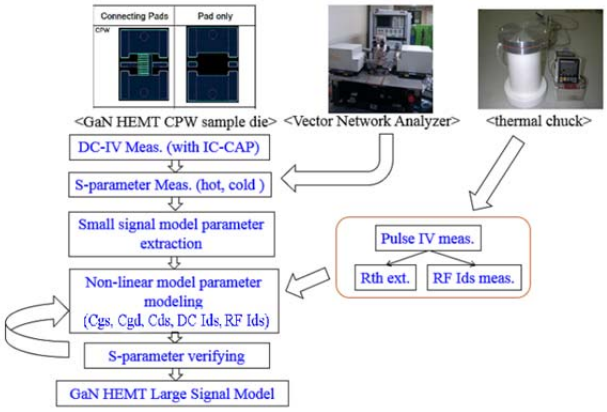


Fig. 2. Angelov model-based GaN HEMT large-signal modeling procedures.

sample dies of GaN HEMT, provided by the foundry service, are used as DUTs. The *S*-parameter is then measured by a vector network analyzer (VNA). The extrinsic parameters and intrinsic parameters are extracted separately by performing hot and cold measurements, respectively. The small-signal model parameters are then extracted from the measured *S*-parameters according to multiple biases. Nonlinear large-signal model parameters, such as gate-source capacitances ($C_{gs}$), gate-drain capacitances ($C_{gd}$), drain-source capacitance ($C_{ds}$), DC $I_{ds}$, and RF $I_{ds}$, are modeled by Angelov model-based tangent-hyperbolic equations. In addition, the thermal effect is reflected by performing a pulsed IV measurement using a DIVA D265 instrument and a thermal chuck. A thermal resistance ($R_{th}$) is extracted using the pulsed IV measurement method [8]. The DC $I_{ds}$ is fitted, including the extracted $R_{th}$, to represent negative current slopes by the thermal effect under high drain voltage and high drain current regions. The RF $I_{ds}$ is measured under a quiescent bias condition and fitted to the RF $I_{ds}$ equa-

Table 1. Model parameters in nonlinear drain current equations of 6 × 125 μm GaN HEMTs

| | DC | RF | | DC | RF |
|---|---|---|---|---|---|
| $I_{pk0}$ (A) | 0.35 | 0.308 | $A_2$ | 0.228 | 0.208 |
| $TCI_{pk0}$ | 0.0024 | -0.002 | $P_{21}$ | 0.636 | 0.390 |
| $P_1$ | 0.013 | 0.047 | $P_{22}$ | 0.006 | 0.745 |
| $TCP_1$ | 0.152 | 0.004 | $P_{31}$ | 0.128 | 0.081 |
| $B_1$ | 1.45 | 1.37 | $P_{32}$ | 0.784 | 0.216 |
| $B_2$ | 0.155 | 0.054 | $V_{gsta}$ | 4.42 | 4.26 |
| $V_{pks}$ (V) | 3.40 | 3.99 | $T_0$ (K) | 290 | 388 |
| $DV_{pks}$ (V) | 0.0001 | 0.6744 | $R_{th}$(℃/W) | 35.8 | 35.8 |
| $A_1$ | 0.002 | 0.000 | $C_{th}$ (μF) | 1.0 | 1.0 |

tions. An initially-equipped large-signal model is verified by comparison with the measured DC $I_{ds}$, RF $I_{ds}$, and $S$-parameters. Finally, the complete model is optimized by some iterations of the above procedures. The size of the GaN HEMT for large-signal modeling is selected as 6 (fingers) × 125 μm (gate width) under the criteria of $F_{max}$ over 20 GHz and load pull power over 34 dBm from 6 to 18 GHz. The extracted $I_{ds}$ model parameters are summarized in Table 1.

Fig. 3 shows a comparison of the DC–IV curves between the measurements and the models, measured at drain voltages ($V_{ds}$) of 0 to 36 V and gate-source voltages ($V_{gs}$) of −3.6 to −1.6 V. The in-house model shows better agreement with the measured data than is observed with the model provided by the foundry service. Fig. 4 shows an RF $I_{ds}$ according to temperature. Under 24 V of a quiescent drain voltage ($V_{dsq}$) and −2.0 V of a quiescent gate voltage ($V_{gsq}$), a pulsed $I_{ds}$ is measured and an RF $I_{ds}$ equation is fitted. The pulse width is 200 ns. The in-house model predicts a reduced RF $I_{ds}$ when temperature increases.

Fig. 5 represents the comparison between the measured $S$-parameters and the simulated $S$-parameters from 0.5 to 60 GHz. As shown in Fig. 5, the in-house model shows better agreement with the measured data up to high frequencies at $S_{22}$ when compared to the model provided by the foundry service. This results from the exact RF $I_{ds}$ modeling by the pulsed IV measurement. Finally, a load pull data at 10 GHz is compared between the measurement and the model. As shown in Fig. 6, the in-house model predicts a more realistic output power than is obtained with the model provided by the foundry service. This result confirms the validity of our large-signal model that includes a thermal model.

## III. Design of a Reactive Matched GaN PA

A reactive matched PA is a type of wideband power amplifier that has an octave bandwidth. It purposely decreases the Q-

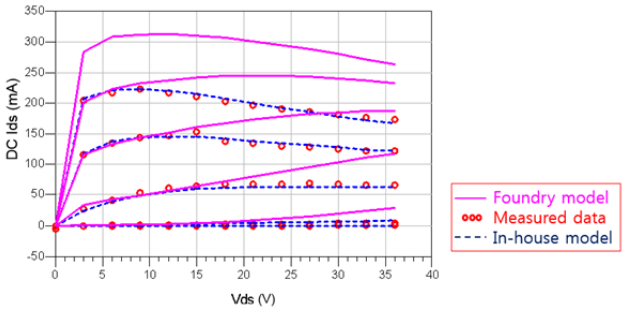


Fig. 3. Comparison of DC–IV curves between measurements and models (GaN HEMT 6 × 125 μm; $V_{ds}$ 0 to 36 V; $V_{gs}$ −3.6 to −1.6 V).

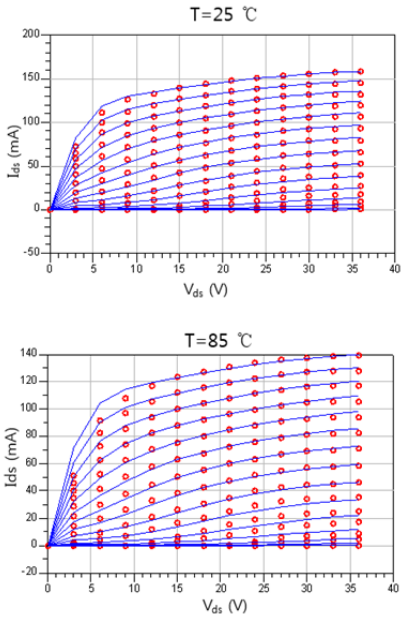


Fig. 4. RF $I_{ds}$ according to temperature (GaN HEMT 6 × 125 μm; $V_{dsq}$ 24 V; $V_{gsq}$ −2.0 V; solid, model; circle, measurement).

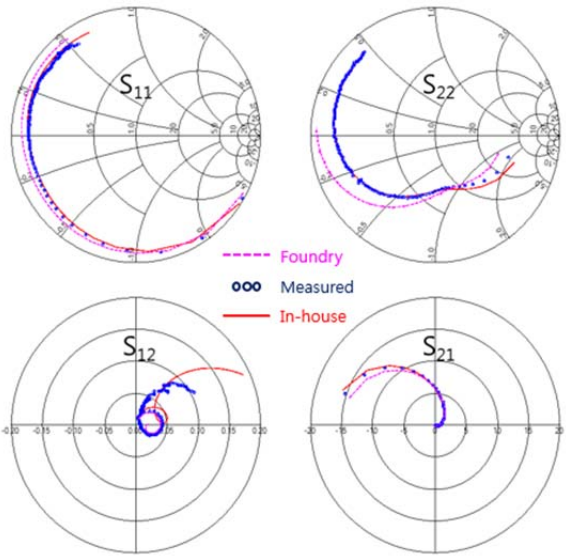


Fig. 5. Comparison of $S$-parameters between measurements and models (GaN HEMT 6 × 125 μm; $V_{ds}$ 24 V; $V_{gs}$ −2.0 V; frequency range, 0.5–60 GHz).

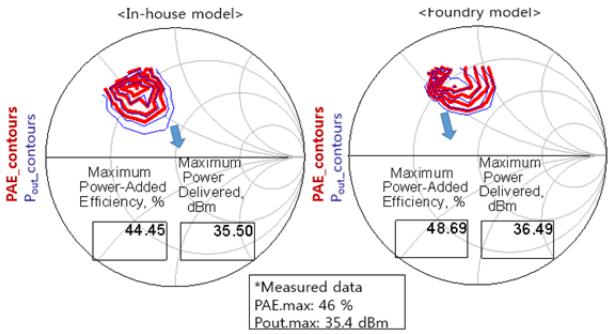


Fig. 6. Comparison of the optimum load pull contour at 10 GHz (GaN HEMT × 125 μm; $V_{ds}$ 28 V; $I_{ds}$ 70 mA; $P_{in}$ 24 dBm).

factors by inserting lossy matching components at the gate of the transistors [11−14]. This approach improves the gain bandwidth, while sacrificing peak gain, peak output power, and power efficiency. However, obtaining the wideband output power requires an additional circuit topology in the reactive matched PA design.

Fig. 7 shows the simulated load pull contour of the 6 × 125 μm GaN HEMTs according to frequencies. As shown in Fig. 7, when the operating frequency increases, the load pull contour rotates in a counterclockwise direction on the Smith chart. Unfortunately, the general output load impedances rotate in the clockwise direction on the Smith chart according to frequencies, which causes the output power characteristics to be very frequency dependent. This prevents the usual PAs from generating uniformly high output power over a wide bandwidth.

We reduce these mismatches between the optimum loads and the output impedances by adopting the L-C resonance technique in the output load matching circuit [15]. First, we set the resonance frequency (in this case, 12 GHz) in the middle of the operating frequency region.

The appropriate value of L and C for resonance is then designed, taking into consideration the length of the micro-strip lines and the size of metal insulator metal (MIM) capacitors. If the capacitance is too large, the power gain will decrease steeply at high frequencies. On the contrary, if the inductance is too large, the layout will be bulky and the MIM capacitors will be

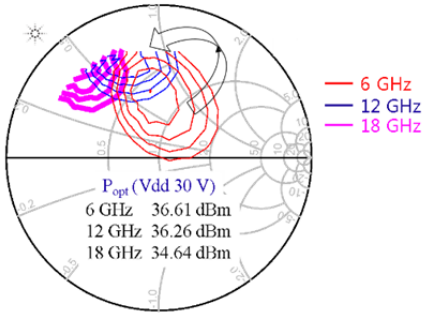


Fig. 7. Simulated load pull contour of 6 × 125 μm GaN HEMTs according to frequencies.

too small to be implemented. In this work, the selected values of L and C are 600 pH and 330 fF, respectively. The output load matching circuits are implemented by the distributed L-C components. The distributed L-C components are repeatedly put close behind the output transistors and after combining the two-unit PAs. Micro-strip lines (50 μm wide and 300 μm long) are used as a distributed inductance of about 150 pH. The MIM capacitors (30 μm × 30 μm) are used as a distributed capacitance of about 230 fF. The distributed L-C components bring about a lower Q than is obtained with lumped L-C components [16]. In addition, the use of micro-strip lines of widths, ranging from 20 to 100 μm according to the output load matching section, mitigates the frequency-sensitive output load variation. Both the L-C resonance and distributed components decrease the variation of the output load impedance according to frequencies. Therefore, these methods can bring about a greater improvement in the wideband output power characteristics. The circuit schematic of a two-stage reactive matched PA with the distributed L-C loads is shown in Fig. 8(a). Fig. 8(b) compares the output impedance under the distributed L-C load with the output impedance under the lumped L-C load on the Smith chart. The output impedance under the distributed L-C load passes through a lower Q region that is relatively closer to the optimum loads than it does when a lumped L-C load is

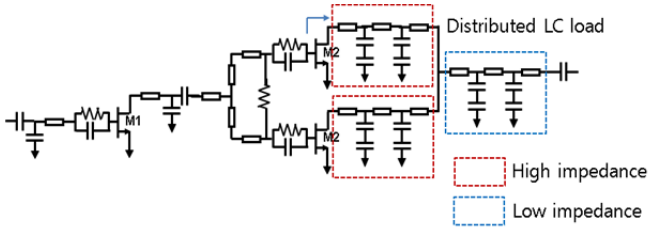


(a)

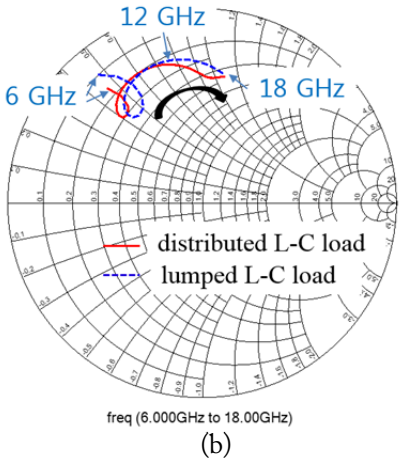


(b)

Fig. 8. (a) Circuit schematic of a two-stage reactive matched GaN power amplifier with the distributed load. (b) Comparison of the output impedance looking into M2 between the distributed L-C load and the lumped L-C load.

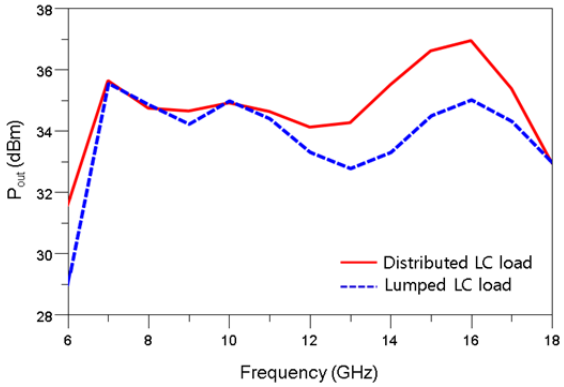


Fig. 9. Comparison of the output power between 2-stage power amplifiers with the distributed L-C load and 2-stage PAs with the lumped L-C load.

applied. Therefore, as shown in Fig. 9, the PAs with the distributed L-C load bring about higher output power than is seen with the lumped L-C load through the wideband frequency region.

## IV. Experimental Results

The proposed PA MMIC has been fabricated by a commercial 0.25 μm GaN process. Fig. 10(a) and (b) show the circuit schematic and the chip photograph. The proposed GaN PA is designed as a three-stage reactive matched type. The GaN HEMTs (6 × 125 μm) are commonly used in the drive and main power stage. The output stage consists of the distributed L-C output load matching circuits of Fig. 8(a) and a Wilkinson power combiner.

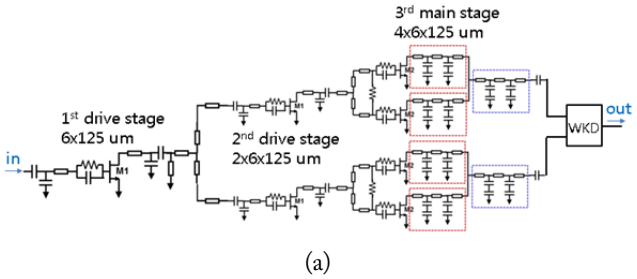


(a)

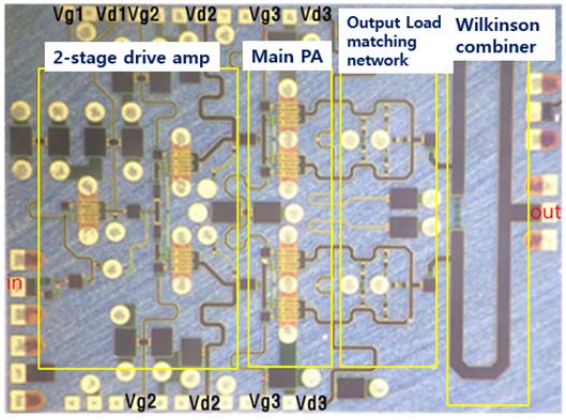


(b)

Fig. 10. (a) Circuit schematic of the GaN power amplifier. (b) Chip photograph of the GaN power amplifier (chip size, 3.8 mm × 2.7 mm).

Figs. 11(a) and (b) compare the measured small-signal *S*-parameters with the simulation. The proposed PA represents the small-signal gain of about 20 dB from 6 to 18 GHz. We presume that errors in the electro-magnetic simulation about the passive components cause partial differences between the simulation and the measurement. Although partial disagreement is evident, the simulation shows reasonable agreement with the measurements from 6 to 18 GHz.

Fig. 12 depicts the measurements of the continuous wave (CW) output power ($P_{out}$) and the power-added efficiency (PAE) according to frequencies. Bias voltages supplied at the PA are optimized to obtain the best $P_{out}$ and PAE. The drastic drop in $P_{out}$ and PAE at 18 GHz, as shown in Fig. 8, is compensated by slightly changing the final output matching circuit by frequency shifting of the minimum $P_{out}$ and PAE (13 to 15 GHz). The proposed GaN PA generates the average CW

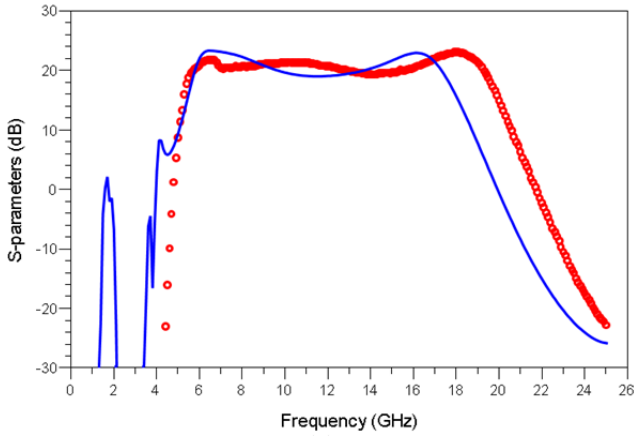


(a)

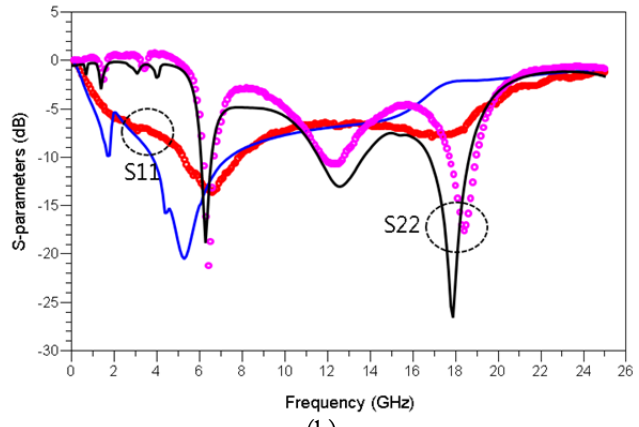


(b)

Fig. 11. Measured *S*-parameter result of the power amplifier: (a) $S_{21}$ and (b) $S_{11}$, $S_{22}$ ($V_{d1}$, $V_{d2}$, $V_{d3}$ = 27 V; $V_{g1}$, $V_{g2}$, $V_{g3}$ = −2.4 V; solid lines, simulation; dot lines, measurement).

Table 2. Performance comparison table of GAN reactive matched power amplifiers

| Ref. | Frequency (GHz) | Topology | Process | PAE (%) | Pout (W) | Gain (dB) | Area ($mm^2$) | Power density ($W/mm^2$) |
|---|---|---|---|---|---|---|---|---|
| [8] | 6–18 | RMPA[a] | 0.25-μm GaN | 14–24 | 3.2–20 | 17–28 | 19.25 | 0.17–1.04 |
| [9] | 8–18 | RMPA | 0.25-μm GaN | 25–35 | 1.25–2 | 7–9 | 10.44 | 0.12–0.19 |
| [10] | 6–18 | RMPA | 0.25-μm GaN | 13–25 | 6–10 | 18–24 | 19.8 | 0.30–0.51 |
| [11] | 6–18 | RMPA | 0.25-μm GaN | 15 | 20 | 9.6 | 19.2 | 1.04 |
| [11] | 6–18 | RMPA | 0.25-μm GaN | 19 | 15.1 | 9.3 | 19.2 | 0.79 |
| This work | 6–18 | RMPA | 0.25-μm GaN | 7.6–23.7 | 3.8–8.4 | 19.4–23.0 | 10.26 | 0.37–0.81 |

[a] Reactive matched power amplifier.

$P_{out}$ of 5.5 W from 6 to 18 GHz. The measured PAE is about 7.6–23.7% from 6 to 18 GHz. The measured peak $P_{out}$ and PAE are 39.2 dBm and 23.7%, respectively, at 7 GHz.

The $P_{out}$ obtained by the simulation using the in-house large-signal models is also compared with the measured $P_{out}$ in Fig. 12. According to the frequencies, the simulated $P_{out}$ is underestimated by 0.0–1.7 dB. As in the *S*-parameter result, the accuracy errors in the electromagnetic simulation with respect to passive components influence the prediction of $P_{out}$. The modeled $R_{th}$ is extracted under the on-wafer condition. In practice, however, the PA is tested under modules in which MMICs are pasted onto a copper jig with gold-tin materials. Thus, the $R_{th}$ in our GaN HEMT model should be decreased. Compensation of these errors in the PA design should improve the prediction inaccuracy. Some inaccuracy remains, but the proposed large-signal model gives a better prediction of $P_{out}$ than that provided by the foundry service.

Table 2 compares the performance of reactive matched GaN PA MMICs. The 0.25-μm GaN process used in this work shows a lower $F_{max}$, and a poorer load pull power and power efficiency than was obtained with the 0.25-μm GaN processes used in other work [17]. However, the proposed GaN PA shows competitive performance to that obtained in state-of-the-art work. In particular, this work achieves excellent performance in power density when compared to the reported RMPAs.

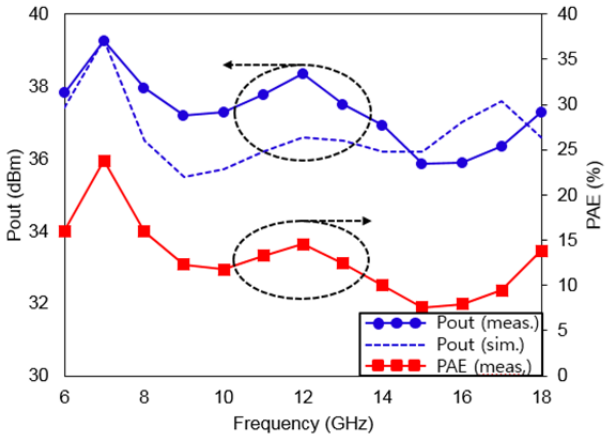


Fig. 12. Measured output power and PAE of the proposed GaN power amplifiers according to frequencies ($V_{d1}$ = 20 V; $V_{d2}$=24 V; $V_{d3}$ = 28 V; $V_{g1}$ = −2.3 V; $V_{g2}$ = $V_{g3}$ = –1.8 V; CW $P_{in}$ = 29–31 dBm).

## V. Conclusion

We implemented 6–18 GHz wideband GaN power amplifiers using a GaN HEMT large-signal model that incorporates a thermal model and is based on various measurements. The in-house GaN HEMT model is effectively used to design a reactive matched PA up to frequencies close to the device's $F_{max}$. The output load matching circuits are implemented by the distributed L-C components. The output load matching using distributed L-C components decreases the variation in the output load impedance according to frequency. The use of GaN HEMTs with high breakdown voltages and RMPAs with the distributed L-C output load matching successfully achieved an output power over 5 W through the octave bandwidth.

The authors gratefully acknowledge the support from the Electronic Warfare Research Center at Gwangju Institute of Science and Technology (GIST), originally funded by the Defense Acquisition Program Administration (DAPA) and the Agency for Defense Development (ADD).

## References

[1] Y. M. Shin, A. Baig, L. R. Barnett, W. C. Tsai, and N. C. Luhmann, "System design analysis of a 0.22-THz sheet-beam traveling-wave tube amplifier," *IEEE Transactions on Electron Devices*, vol. 59, no. 1, pp. 234–240, Jan. 2012.

[2] A. R. Gilmour, *Microwave Tubes*, Boston, MA: Artech House, 1986.

[3] A. Katz, B. Eggleston, and J. MacDonald, "GaN SSPA for UHF space applications," in *Proceedings of IEEE MTT-S International Microwave Symposium Digest*, Seattle, WA, 2013, pp. 1–4.

[4] B. M. Green, V. Tilak, S. Lee, H. Kim, J. A. Smart, K. J. Webb, J. R. Shealy, and L. F. Eastman, "High-power broad-band AlGaN/GaN HEMT MMICs on SiC substrates," *IEEE Transactions on Microwave Theory and Techniques*, vol. 49, no. 12, pp. 2486–2491, Dec. 2001.

[5] S. Nuttinck, E. Gebara, J. Laskar, and H. M. Harris, "Study of self-heating effects, temperature-dependent modeling, and pulsed load-pull measurements on GaN HEMTs," *IEEE Transactions on Microwave Theory and Techniques*, vol. 49, no. 12, pp. 2413–2420, Dec. 2001.

[6] I. Angelov, H. Zirath, and N. Rosman, "A new empirical nonlinear model for HEMT and MESFET devices," *IEEE Transactions on Microwave Theory and Techniques*, vol. 40, no. 12, pp. 2258–2266, Dec. 1992.

[7] L. S. Liu, J. G. Ma, and G. I. Ng, "Electrothermal large-signal model of III–V FETs including frequency dispersion and charge conservation," *IEEE Transactions on Microwave Theory and Techniques*, vol. 57, no. 12, pp. 3106–3117, Dec. 2009.

[8] Keysight Technologies, "Angelov_Model (Angelov (Chalmers) Nonlinear GaAsFET Model)," 2013; http://eda-docs.software.keysight.com/pages/viewpage.action?pageId=39817918.

[9] I. Angelov, L. Bengtsson, and M. Garcia, "Extensions of the Chalmers nonlinear HEMT and MESFET model," *IEEE Transactions on Microwave Theory and Techniques*, vol. 44, no. 10 , pp. 1664–1674 , Oct. 1996.

[10] J. Joh, J. A. del Alamo, U. Chowdhury, T. M. Chou, H. Q. Tserng, and J. L. Jimenez, "Measurement of channel temperature in GaN high-electron mobility transistors," *IEEE Transactions on Electron Devices*, vol. 56, no. 12, pp. 2895–2901, Dec. 2009.

[11] U. Schmid, H. Sledzik, P. Schuh, J. Schroth, M. Oppermann, P. Bruckner, F. van Raay, R. Quay, and M. Seelmann-Eggebert, "Ultra-wideband GaN MMIC chip set and high power amplifier module for multi-function defense AESA applications," *IEEE Transactions on Microwave Theory and Techniques*, vol. 61, no. 8, pp. 3043–3051, Aug. 2013.

[12] Y. Niida, Y. Kamada, T. Ohki, S. Ozaki, K. Makiyama, N. Okamoto, M. Sato, S. Masuda, and K. Watanabe, "X-Ku wide-bandwidth GaN HEMT MMIC amplifier with small deviation of output power and PAE," in *Proceedings of IEEE Compound Semiconductor Integrated Circuit Symposium (CSICs)*, La Jolla, CA, 2014, pp. 1–4.

[13] G. Mouginot, Z. Ouarch, B. Lefebvre, S. Heckmann, J. Lhortolary, D. Baglieri, et al., "Three stage 6–18 GHz high gain and high power amplifier based on GaN technology," in *Proceedings of IEEE MTT-S International Microwave Symposium Digest*, Anaheim, CA, 2010, pp. 1392–1395.

[14] E. Kuwata, K. Yamanaka, H. Koyama, Y. Kamo, T. Kirikoshi, M. Nakayama and Y. Hirano, "C-Ku band ultra broadband GaN MMIC amplifier with 20W output power," in *Proceedings of Asia-Pacific Microwave Conference (APMC)*, Melbourne, Australia, 2011, pp. 1558–1561.

[15] E. Kuwata, K. Yamanaka, T. Kirikoshi, A. Inoue, and Y. Hirano, "C-Ku band 120% relative bandwidth high efficiency high power amplifier using GaN HEMT," in *Proceedings of Asia-Pacific Microwave Conference (APMC)*, Singapore, 2009, pp. 1663–1666.

[16] D. M. Pozar, *Microwave Engineering*, 4th ed., New York, NY:Wiley, 2012.

[17] S. Lee, H. Park, J. Kim, and Y. Kwon, "A 6-18 GHz GaN pHEMT power amplifier using non-foster matching," in *Proceedings of IEEE MTT-S International Microwave Symposium Digest*, Phoenix, AZ, 2015, pp. 1–4.

Jihoon Kim

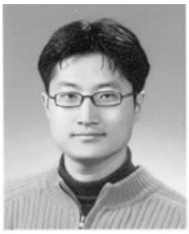

was born in Korea, and received the B.S. degree in electrical engineering from Seoul National University, Seoul, Korea, in 2003. He is working toward the Ph.D. degree in electrical engineering at Seoul National University. His research activities include the design of millimeter wave integrated circuits using GaN, GaAs, and Si devices and the modeling of FETs such as GaAs pHEMTs, CMOS, and GaN HEMTs.

Kwangseok Choi

received the B.S. and M.S. degree in electrical engineering from Sogang University, Seoul, Korea, in 2008 and 2010, respectively, and is currently working toward the Ph.D. degree in electric and computer engineering at Seoul National University. From 2010 to 2013, he was with Gigalane, Suwon, Korea, as a Research Engineer. From 2013 to 2014, he joined the System Integrated Circuit Laboratory, LG Electronics, Seoul, Korea, as a Junior Research Engineer.

## Sangho Lee

received the B.S. degree in electrical engineering from Seoul National University, Seoul, Korea, in 2011, and is working toward the Ph.D. degree in electrical and computer engineering at Seoul National University. His research activities include millimeter-wave/RF integrated circuits and system design for wireless communication and RADAR, especially high power and broadband PAs design.

## Hongjong Park

received the B.S. degree in electrical and computer engineering from Seoul National University, Seoul, Korea, in 2012, and is working toward the Ph.D. degree in electrical and computer engineering at Seoul National University. His research interests include large-signal modeling of GaN HEMTs and millimeter-wave GaN MMICs.

## Youngwoo Kwon

received the B.S. degree in electronics engineering from Seoul National University, Seoul, Korea, in 1988, and the M.S. and Ph.D. degrees in electrical engineering from The University of Michigan at Ann Arbor, Ann Arbor, MI, USA, in 1990 and 1994, respectively. From 1994 to 1996, he was with the Rockwell Science Center, as a Member of Technical Staff, where he was involved in the development of millimeter-wave monolithic integrated circuits (ICs). In 1996, he joined the faculty of the School of Electrical Engineering, Seoul National University, where he is currently a Professor. He is a co-inventor of the switchless stage-bypass power amplifier architecture "CoolPAM." He co-founded Wavics, a power amplifier design company, which is now fully owned by Avago Technologies. In 1999, he was awarded a Creative Research Initiative Program grant by the Korean Ministry of Science and Technology to develop new technologies in the interdisciplinary area of millimeter-wave electronics, MEMS, and biotechnology. He has authored or coauthored over 150 technical papers in internationally renowned journals and conferences. He holds over 20 patents on RF MEMS and power amplifier technology. Dr. Kwon has been an associate editor for the IEEE Transactions on Microwave Theory and Techniques. He has also served as a Technical Program Committee member of various microwave and semiconductor conferences, including the IEEE International Microwave Symposium (IMS), RF Integrated Circuit (RFIC) Symposium, and the International Electron Devices Meeting (IEDM). Over the past years, he has directed a number of RF research projects funded by the Korean Government and U.S. companies. He was the recipient of a Presidential Young Investigator Award from the Korean Government in 2006.